Electronic Supplementary Material (ESI) for Journal of Materials Chemistry C.
This journal is © The Royal Society of Chemistry 2024

Supporting Information

Ultrafast Scintillation at Room Temperature Achieved on $CsPbCl_3$-based Single Crystal through Br Over-doping

Yulin Zhang,[a,b,c] Meng Shen,[a,b,c] Bingliang Cheng,[b,c] Wenjuan Ma,[b,c] Xiaole Huang,[b,c] Lei Zhang, [b,c] Zhifang Chai,[b,c] Wenwen Lin*[b,c]

a. School of Materials Science and Chemical Engineering, Ningbo University, Ningbo 315211, China

b. Zhejiang Key Laboratory of Data-Driven High-Safety Energy Materials and Applications, Ningbo Key Laboratory of Special Energy Materials and Chemistry, Ningbo Institute of Materials Technology and Engineering, Chinese Academy of Sciences, Ningbo 315201, China

c. Qianwan Institute of CNITECH, Ningbo 315336, China

*Corresponding author. Email: linwenwen@nimte.ac.cn

Experimental section

Materials

Chemicals were used as obtained: cesium chloride (99.99% purity, Aladdin), lead chloride (99.99% purity, Aladdin), CsBr (99.99% purity, Aladdin), liquid bromine (99.5% purity, Hushi).

$CsBr_3$ decomposes into CsBr and Br_2 vapor upon heated at above 120 °C,[1] therefore $CsBr_3$ is used as the source releasing Br_2 vapor as dopant. The $CsBr_3$ powder was synthesized in a fume hood. First, the CsBr powder (0.047-0.142 g, 2.231×10^{-4}-6.693×10^{-4} mol) was mixed with excess liquid bromine (0.035-0.106 g, 2.231×10^{-4}-6.693×10^{-4} mol), subsequently, the mixture was loaded into a round-bottled flask. The flask was soaked in an oil bath at 80 °C for 1 hour to ensure the complete reaction of $CsBr + Br_2 = CsBr_3$. After all the excess liquid Br_2 vaporized, the orange final product left in the bottom of the flask was collected. The PXRD pattern of the orange substance confirmed that it was of pure phase $CsBr_3$, as shown in Figure S1.

Crystal growth and methods

(1) First, the inner wall of the silica ampoule was rinsed with acetone. Second, the outer wall of ampoule was burned by flame until a shiny carbon film forms on the inner wall due to the carbonization of acetone. Finally, the ampoule was rinsed and cleaned with deionized water.

(2) The mixture of all raw materials (CsCl, 11.313 g, 6.720×10^{-2} mol, $PbCl_2$, 18.687 g, 6.720×10^{-2} mol) were loadedinto the above-mentioned silica ampoules to synthesize pure-phase $CsPbCl_3$. Subsequently, the ampoules were flame-sealed under continuous pumping at a residual pressure of 1×10^{-1} mbar. To ensure complete melting and reaction of raw materials, the ampoules were loaded into a rocking furnace and then soaked at 700 °C for 24 hours, followed by slow cooling to room temperature in 24 hours. The as-synthesized polycrystalline product was of pure phase $CsPbCl_3$, confirmed by the PXRD patterns (Figure 1a).

(3) The polycrystalline $CsPbCl_3$ raw material was loaded into a conical tip and carbon-coated silica ampoule with an ID of 16 mm and an OD of 20 mm, which was customized for the Bridgman crystal growth. In order to introduce Br_2 dopant into $CsPbCl_3$ during crystal growth, silica crucibles (an ID of 7 mm and an OD of 10 mm) were fixed above the raw material in the ampoules to load $CsBr_3$ releasing Br dopant. Figure S2 shows the scheme of the fixed crucible inside the fused ampoule, with two concave pits formed by burning at the middle section for fixation. The Br_2 dopant source $CsBr_3$ (0.083-0.294 g, 2.23×10^{-4}-6.693×10^{-4} mol) was loaded into the silica crucible. The $CsBr_3$ releases Br_2 vapor as a dopant in $CsPbCl_3$, while liquid CsBr (melting point 636 °C) was left in the crucible during the crystal growth process. The conical-tip ampoule was vacuumed and then sealed by flame. $CsPbCl_3$:Br_x (x = 0.006, 0.014, 0.020) crystals were grown by the Bridgman method under

different concentrations of Br atmosphere.[2] The vertical Bridgman furnace is divided into three temperature zones: high-temperature zone (700 °C), medium-temperature zone (600 °C) and low-temperature zone (530 °C), as shown in Figure S4. After crystal growth, the ampoules had no residual orange Br_2 vapor above the crystallized ingot, indicating all the Br_2 vapor had been incorporated into the $CsPbCl_3$ ingot. The white substance left in the crucible was finally confirmed to be the pure phase CsBr, indicated by the PXRD pattern of the white substance (Figure S3).[13] The existence of CsBr suggests the decomposition of Br_2 source $CsBr_3$. An ampoule loaded with pure $CsPbCl_3$ without Br_2 source $CsBr_3$ was prepared at the same time, and then subjected to crystal growth under identical experimental conditions. The as-grown undoped $CsPbCl_3$ ingot was extracted for the control samples for comparison.

Crystal processing and characterization

The powder X-ray diffraction (PXRD) test was carried out on the Bruker D8 Advance instrument with a Cu Kα radiation source (radiation λ = 1.5478 Å), a working voltage of 40 KV, and a working current of 40 mA. The 2 theta ranges from 10 ° to 70 ° with an angle step of 0.02 °. The obtained PXRD patterns were indexed with a simulated pattern to identify phase and phase purity.[3] The ingots were sliced into 2 mm thick slices by cutting perpendicularly to the crystal growth direction. The cutting was done on a SYJ-200 cutting machine equipped with a 200 mm diameter edge-sintered diamond saw blade. The wafers were subjected to rough polishing using 800-1200 grid SiC and papers, and then fine polishing on a polishing cloth using WD-40 as the lubricant.

Rietveld refinement of powder X-ray diffraction patterns

The Bruker software TOPAS was used for Rietveld refinement of powder X-ray diffraction data.[4] This method calculates the powder diffraction pattern using a specific peak shape function based on the initial crystal structure model and parameters provided. The crystal structure and peak shape parameters are continuously adjusted using the least squares method to match the calculated pattern with the experimental pattern, resulting in refined structural parameters.[5]

Scanning Electron Microscope-Energy Dispersive Spectroscopy (SEM-EDS)

The energy-dispersive spectroscopy (EDS, Bruker XFlash Detector equipped in SEM HITACHI Regulus8230) was adopted to identify and quantify the Br element of the grown crystals.

Differential Scanning Calorimetry (DSC)

To assess the thermal stability of $CsPbCl_3$:Br_x (x = 0.006, 0.014, 0.020), differential scanning calorimetry (DSC) analysis was performed by using Netzsch STA449 F3. Approximately 20 mg specimen was uniformly ground, and then loaded into a silica ampoule customized for DSC measurements. The ampoule was flame-sealed until evacuated to 10^{-1} mbar. Meanwhile, an empty silica ampoule was flame-sealed as the control sample. The

sample was heated to 650 °C at a ramp rate of 10 °C·min^{-1} and then cooled at a cooling rate of 10 °C·min^{-1} to room temperature.

Optical Properties Characterization

(1) UV-visible diffuse reflectance spectroscopy

Solid-state diffuse reflectance UV-vis-NIR spectroscopy at 300 K was performed by using HITACHIUH4150 UV Visible spectrophotometer operating in a 200-800 nm wavelength region, and a 30 nm·min^{-1} scanning speed. $BaSO_4$ was used as the reflecting reference standard.

(2) Steady-state photoluminescence spectroscopy

FLS1000 photoluminescence spectrometer equipped with a 375 nm laser was used to acquire steady-state photoluminescence spectra. The crystals were subjected to a photoluminescence test in the emission wavelength range of 400-800 nm.

(3) Time-resolved transient photoluminescence spectra (TRPL)

In order to avoid the disturbance of surface states on PL spectra, cleaved $CsPbCl_3$:Br_x (x = 0.006, 0.014, 0.020) chunks were extracted for PL tests. The time-resolved photoluminescence spectra at room temperature were acquired for $CsPbCl_3$ and $CsPbCl_3$:$Br_{0.020}$ crystals without polishing using the Edinburgh Instruments FLS1000 spectrofluorometer. The spectrofluorometer is equipped with a time-correlated single photon counting (TCSPC) lifetime option and a photomultiplier HS-PMT detector. The $CsPbCl_3$:Br_x (x = 0.006, 0.014, 0.020) crystals were mounted into the sample holder module. The PL of the $CsPbCl_3$:Br_x (x = 0.006, 0.014, 0.020) crystal was excited by a 375 nm laser with a power of 5000 μW. The laser source faces and hits the sample at 45° with a distance of around 10 cm. The emission slit width for detection was set as 2 nm. The PL data was collected from the emission range of 400 to 800 nm with a 1 nm interval and a 0.5 s dwell time. For PL decay time measurement, each decay was fit with a combination of two or three stretched exponentials using the FAST software package.

(4) Temperature-dependent photoluminescence

The low-temperature photoluminescence (PL) spectra were carried out on cleaved $CsPbCl_3$ and $CsPbCl_3$:$Br_{0.020}$ chunks without polishing using the Edinburgh Instruments FLS1000 spectrofluorometer. The samples were mounted on a vertical stage and then cooled down using liquid nitrogen. The PL of the $CsPbCl_3$:Br_x (x = 0.006, 0.014, 0.020) crystal was excited by a 375 nm laser with a power 5000 μW at 100-200 K in the wavelength range of 400-800 nm. Subsequently, a long-pass filter with a 400 nm cut-on wavelength reflects the laser light before the monochromator, and then filters the emission.

Device fabrication and electrical performance characterization

The contacts were fabricated by sputtering Au film on the parallel surfaces of the polished wafer. The sample with Au electrodes was mounted on a 25.40 × 25.40 mm^2 glass slide. The effective contact area on the top of the samples is approximately 22.96~27.25 mm^2. The thickness of the device is about 1.56-1.94 mm. The Cu wires were attached to the

Au contacts and then attached Cu tap at the edge of the glass slide by applying the conductive Ag adhesive. The *I-V* curves in the dark were measured using a KEITHLEY 6517B source meter. Electromagnetic interference and photoconductive responses were eliminated by a metallic enclosure.

Space charge limited current (SCLC) measurement

The dark *I-V* curves using the Keithley 6517B source meter were measured, and then the trap state density was calculated by the SCLC model with the following formula equation:[6]

$$N_{trap} = \frac{2\varepsilon_0 \varepsilon V_{TFL}}{eL^2}$$

Among the equation, ε is the relative dielectric constant, ε_0 is the dielectric constant of the vacuum dielectric constant (8.85×10^{-12} F·m^{-1}), L is the thickness of the crystal, e is the elemental charge, and V_{TFL} is the turning point of Ohmic to the trap-filled region in the *I-V* curves.

Time-resolved transient radioluminescence (RL) spectra measurements

Time-resolved transient RL measurements at room temperature were carried out for freshly cleaved $CsPbCl_3$ and $CsPbCl_3:Br_{0.020}$ crystals without polishing using the Edinburgh instruments FLS1000 spectrofluorometer. The scintillation of the $CsPbCl_3:Br_{0.020}$ single crystal was excited by 5.31 MeV alpha particles from a ^{210}Po isotope with an activity of 0.5 mCi. The radiation source faces and hits the sample at 45° with a distance of around 1 cm. The emission slit width for detection was set as 0.5 nm. The RL data was collected in the emission wavelength range of 400 to 800 nm with a 1 nm interval and a 0.5 s dwell time. More details about the "^{210}Po" radiation source were elaborated at Table S1.

X-ray radioluminescence characterization

X-ray radioluminescence spectra at room temperature were acquired for the cleaved $CsPbCl_3$ and $CsPbCl_3:Br_{0.020}$ chunks without polishing using a Zolix FLS-XrayV series fluorescence spectrometer equipped with a tungsten X-ray target. The emission was filtered by using a long-pass filter with a cut-off wavelength of 400 nm, and then detected by a PMT in the wavelength range of 400-800 nm.

X-ray imaging characterization

The schematic diagram of the X-ray imaging system is shown in Figure 6a. The X-rays are generated from OminiFluo960-XrayP-Z of Zolix equipped with a tungsten target X-ray tube, with a maximum power is 50 W, which can be tuned via changing work current and voltage. Then an integrating sphere was applied to collect RL. The X-ray dose rate was controlled to 25 Sv·h^{-1}, which was calibrated by a radiation dose meter (FLS-AT1121). The X-ray images were captured by a CMOS camera (Tucsen FL-20BW) with a macro lens and a sensor resolution of 20 megapixels. During the measurement, the X-ray shutter was always open. The test-pattern plate is made of 0.03

mm thick lead foil, with a maximum resolution ratio of 20 lp·mm^{-1}. The adopted line pair test pattern is plotted in Figure S12(a).

Table S1. Details about the "^{210}Po" radiation source.

Model P-2042 Specifications	
Isotope	Polonium-210
Material	Aluminium and stainless steel
Emission	Alpha
Activity	5 mCi (185 MBq)
Decay Time	1.2 seconds, 1.5", 1,000 to 100 V

Table S2. Basic properties of commercial scintillation crystals used in PET scanners.

	$LaBr_3$	**GSO**	**LYSO**	**LSO**	**BGO**
Chemical Formula	$LaBr_3$	Gd_2SiO_5	$Lu_{2(1-x)}Y_{2x}SiO_5$	Lu_2SiO_5	$Bi_4Ge_3O_{12}$
Density ($g \cdot cm^{-3}$)	5.3	4.89	7.15	7.4	7.13
Wavelength (nm)	370	440	410	420	480
Decay time (ns)	25	60	≤47	40	300
Hygroscopic?	Yes	No	No	No	No
Reference	7	8	9	10	11

Table S3. Rietveld refinement results of cell parameters for undoped $CsPbCl_3$ and $CsPbCl_3:Br_x$ (x = 0.006, 0.014, 0.020) structures.

Sample	**$CsPbCl_3$**	**$CsPbCl_3:Br_{0.006}$**	**$CsPbCl_3:Br_{0.014}$**	**$CsPbCl_3:Br_{0.020}$**
***a* (Å)**	7.89989±0.00009	7.90200±0.00010	7.90361±0.00008	7.90460±0.00010
***b* (Å)**	7.90161±0.00012	7.90541±0.00012	7.90702±0.00016	7.90819±0.00012
***c* (Å)**	11.24841±0.00012	11.25243±0.00009	11.25382±0.00013	11.25454±0.00009
***V* (Å^3)**	702.15380±0.02356	702.94520±0.03782	703.28660±0.02488	703.53441±0.03306
Crystal system	Orthorhombic	Orthorhombic	Orthorhombic	Orthorhombic
Space group	*Pbnm*	*Pbnm*	*Pbnm*	*Pbnm*

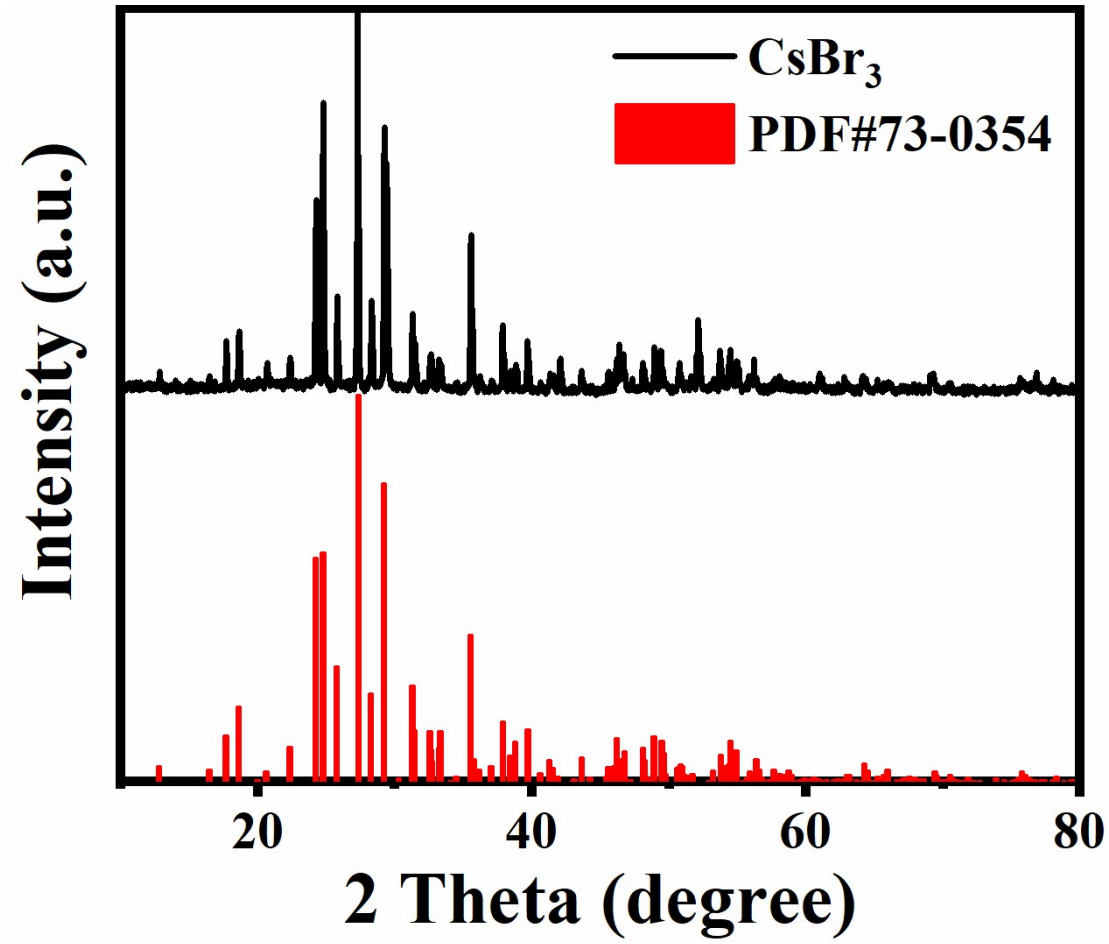

Fig. S1 PXRD pattern of as-synthesized $CsBr_3$.[1]

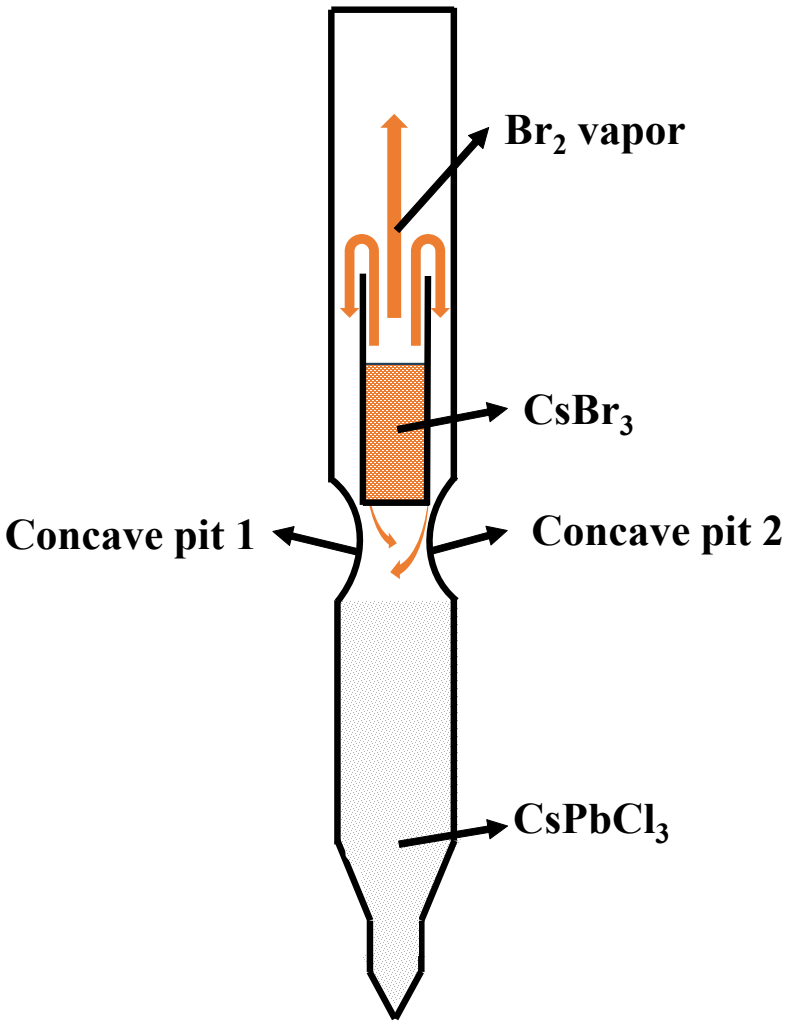

Fig. S2 Scheme of the fixed crucible inside the fused ampoule.

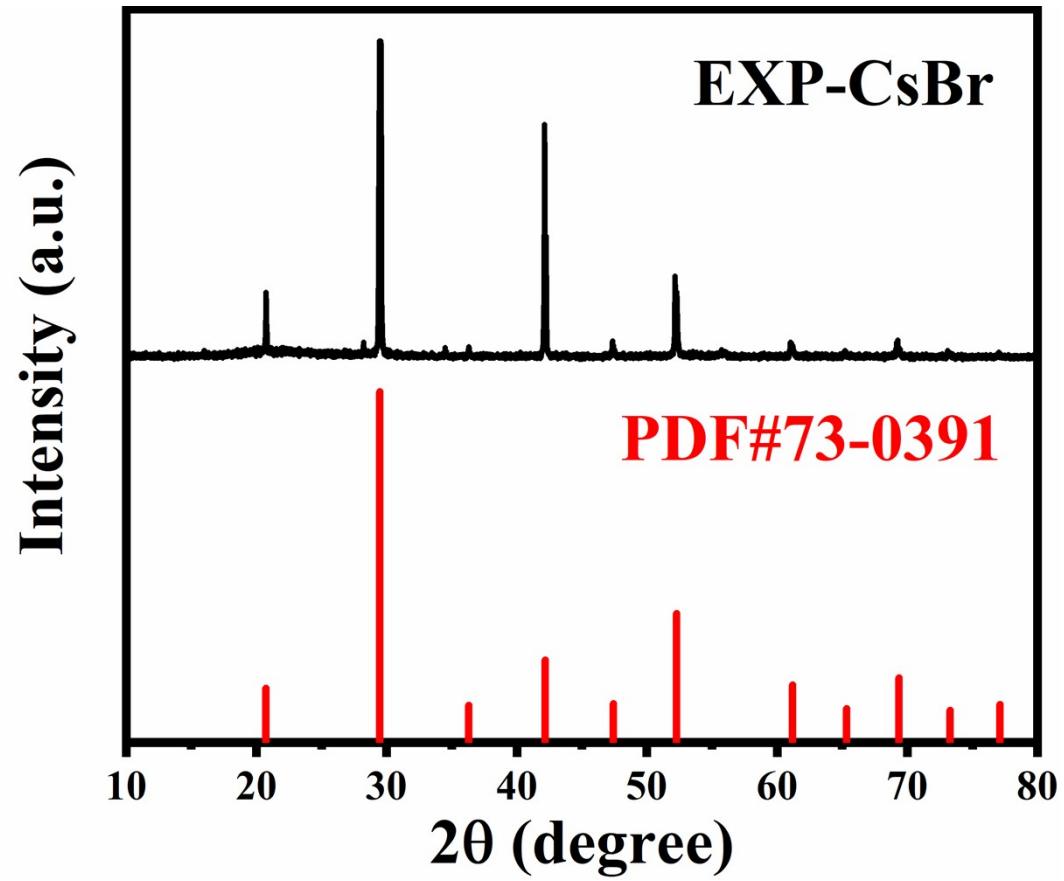

Fig. S3 PXRD pattern of the residual CsBr in the crucible.[12]

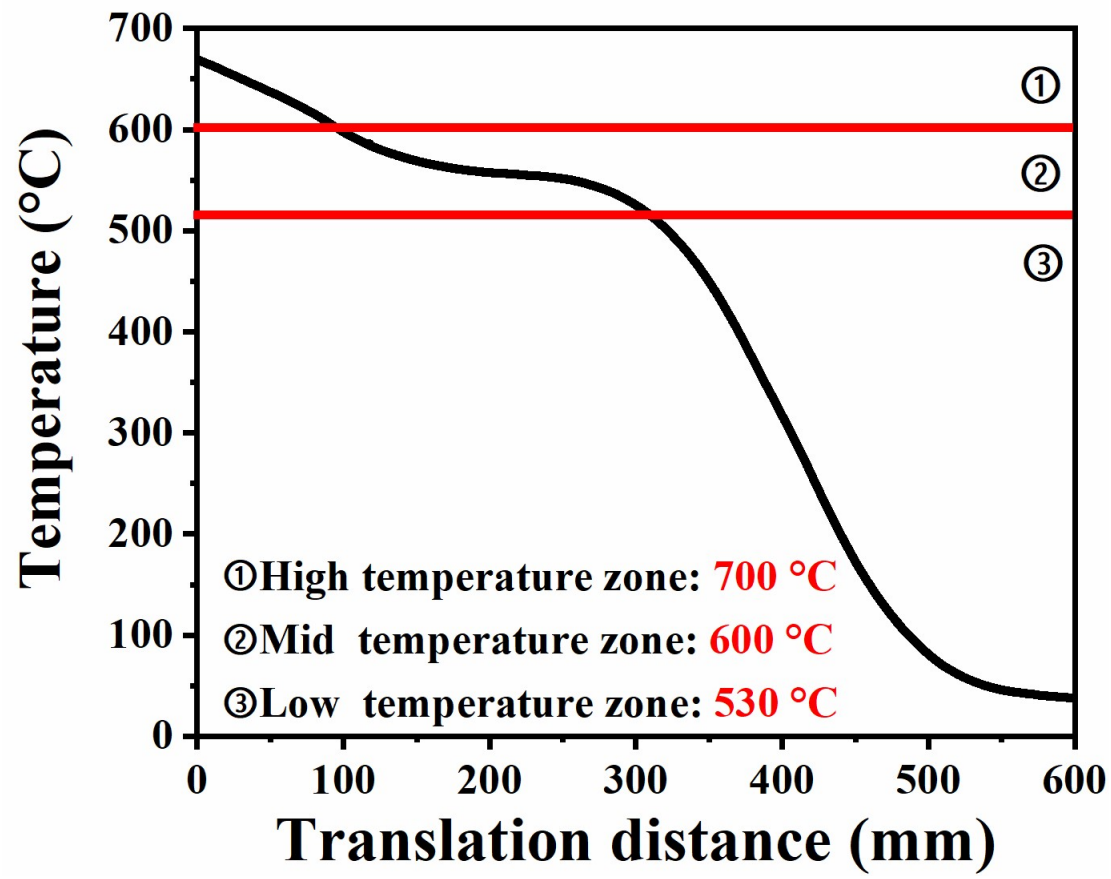

Fig. S4 Bridgman furnace temperature profile, high-temperature zone: 700 °C, middle-temperature zone :600 °C, low-temperature zone: 530 °C.

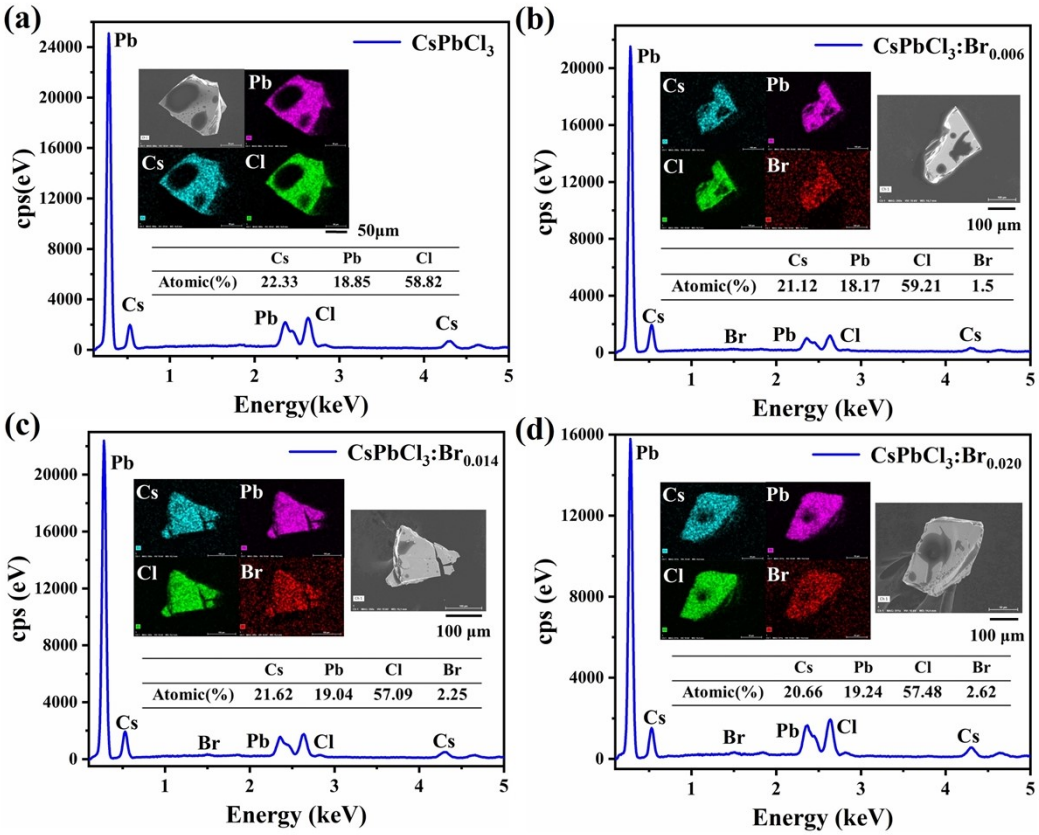

Fig. S5 (a)-(d) Scanning electron microscope-energy dispersive spectrometer (SEM-EDS) testing of the undoped $CsPbCl_3$ and $CsPbCl_3:Br_x$ (x = 0.006, 0.014, 0.020) single crystal.

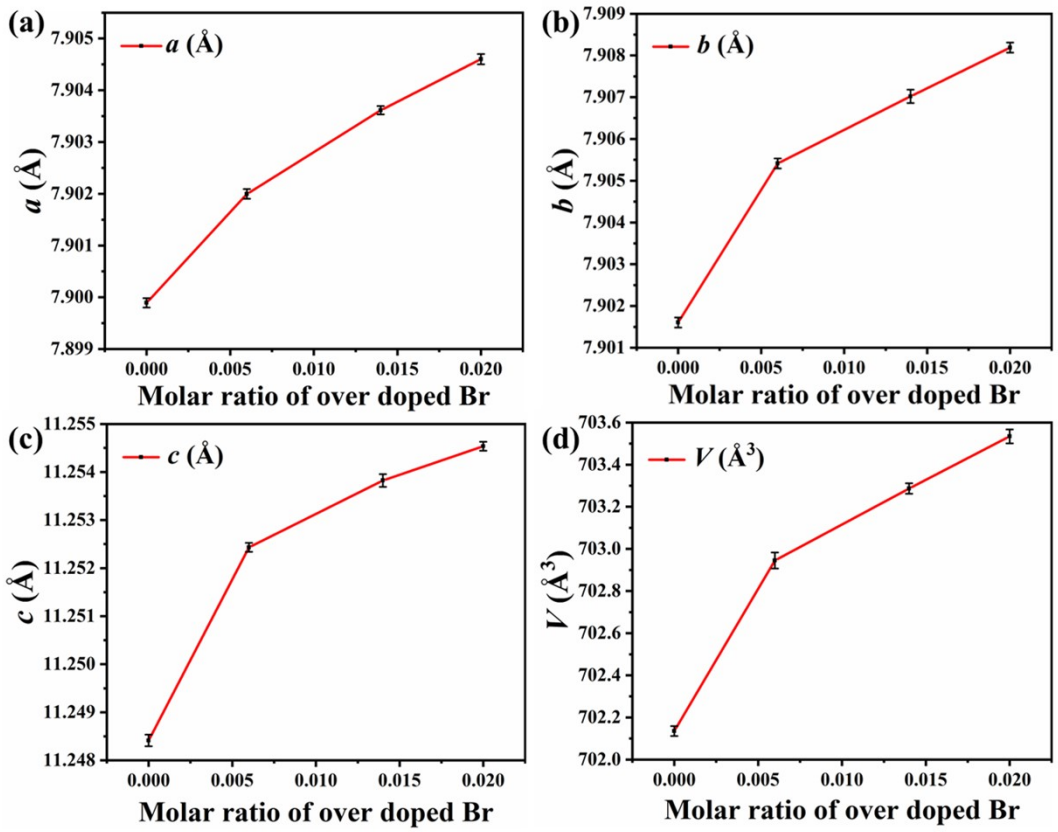

Fig. S6 Lattice constant variation for $CsPbCl_3$ and $CsPbCl_3$:Br_x (x = 0.006, 0.014, 0.020) crystals. (a) Trend of lattice constant "*a*" variation. (b) Trend of lattice constant "*b*" variation. (c) Trend of lattice constant "*c*" variation. (d) Trend of cell volume "*V*" variation.

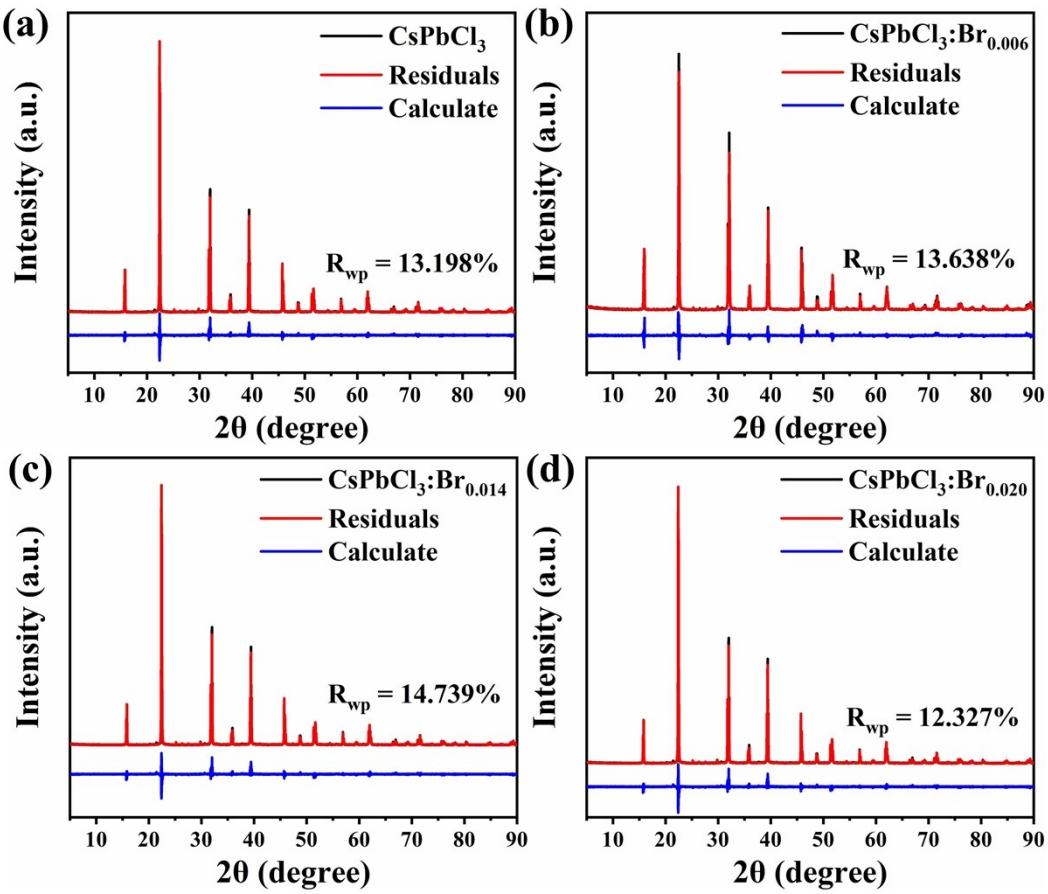

Fig. S7 (a)-(d) Reliability factors of Rietveld refinement of powder X-ray diffraction data of the undoped $CsPbCl_3$ and $CsPbCl_3$:Br_x (x = 0.006, 0.014, 0.020) powder.

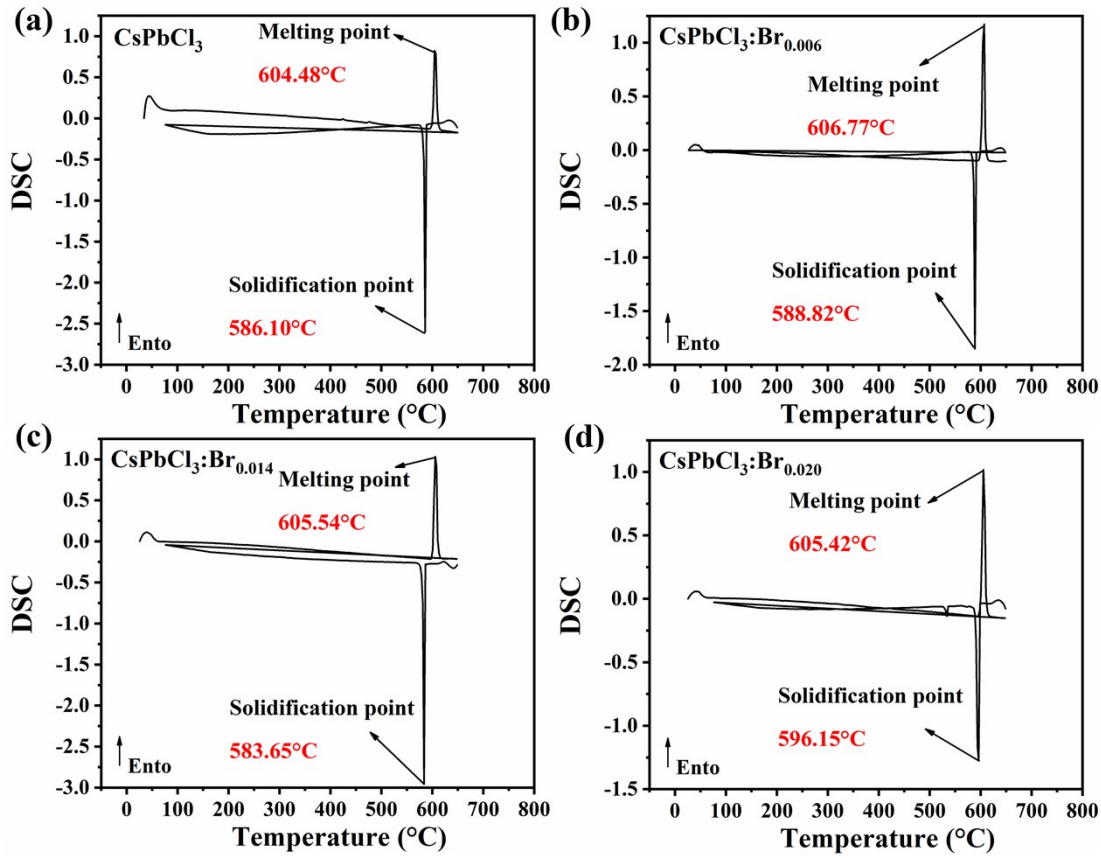

Fig. S8 (a)-(d) Differential Scanning Calorimetry (DSC) curves of the undoped $CsPbCl_3$ and $CsPbCl_3:Br_x$ (x = 0.006, 0.014, 0.020).

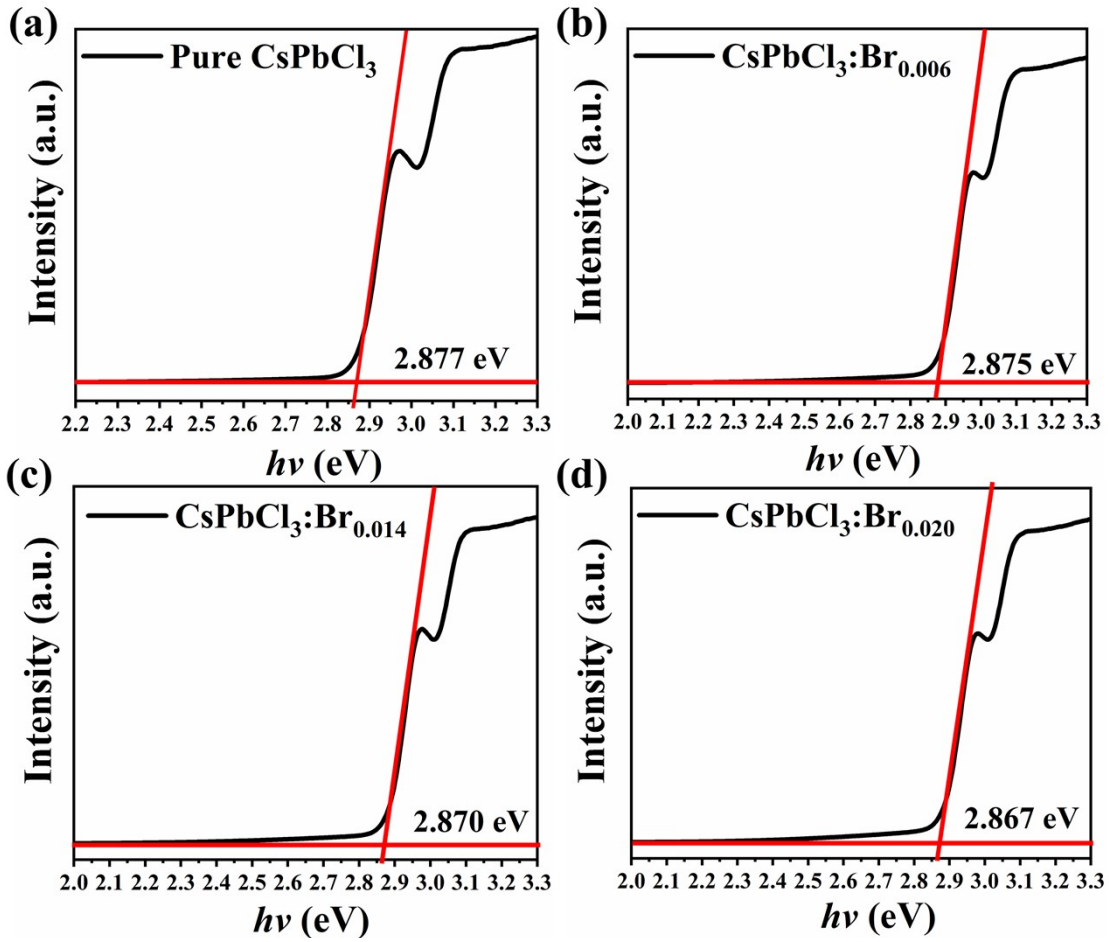

Fig. S9 (a)-(d) The bandgap of the undoped $CsPbCl_3$ crystal and the bandgap of $CsPbCl_3:Br_x$ (x = 0.006, 0.014, 0.020) crystal.

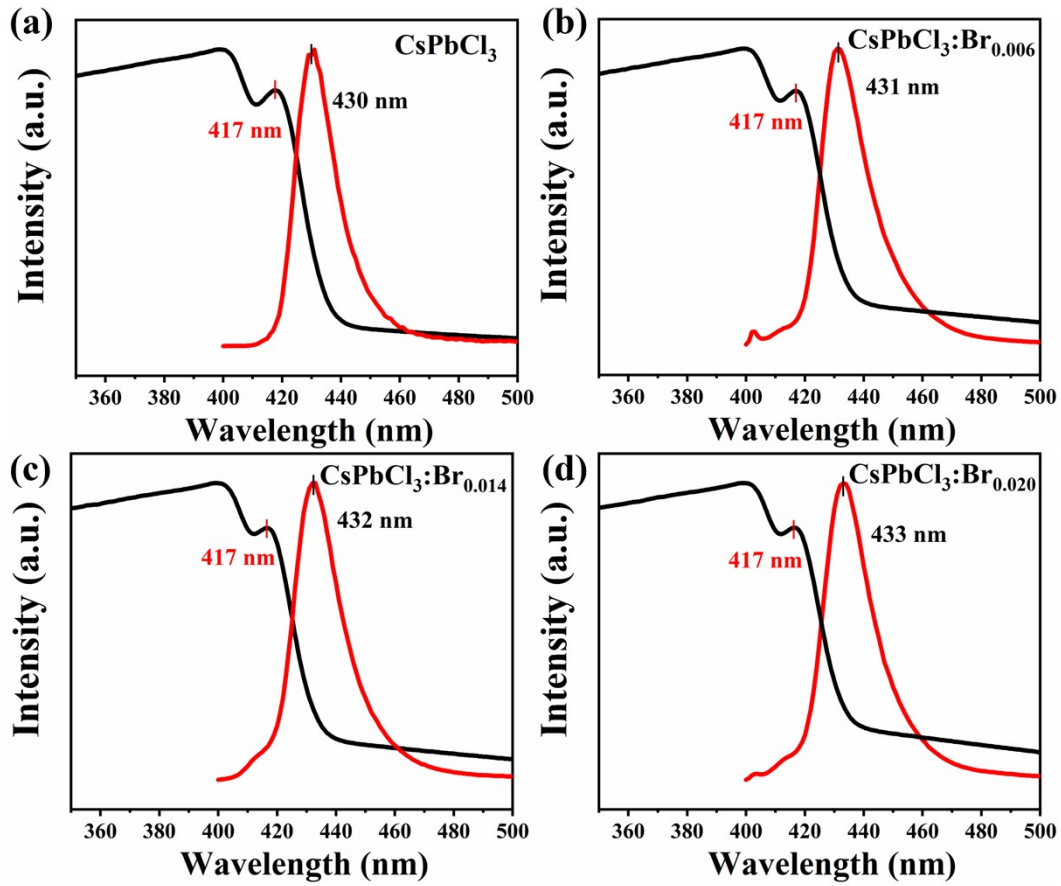

Fig. S10 (a)-(d) Stokes shift diagram of $CsPbCl_3$ and $CsPbCl_3:Br_x$ (x = 0.006, 0.014, 0.020) crystals.

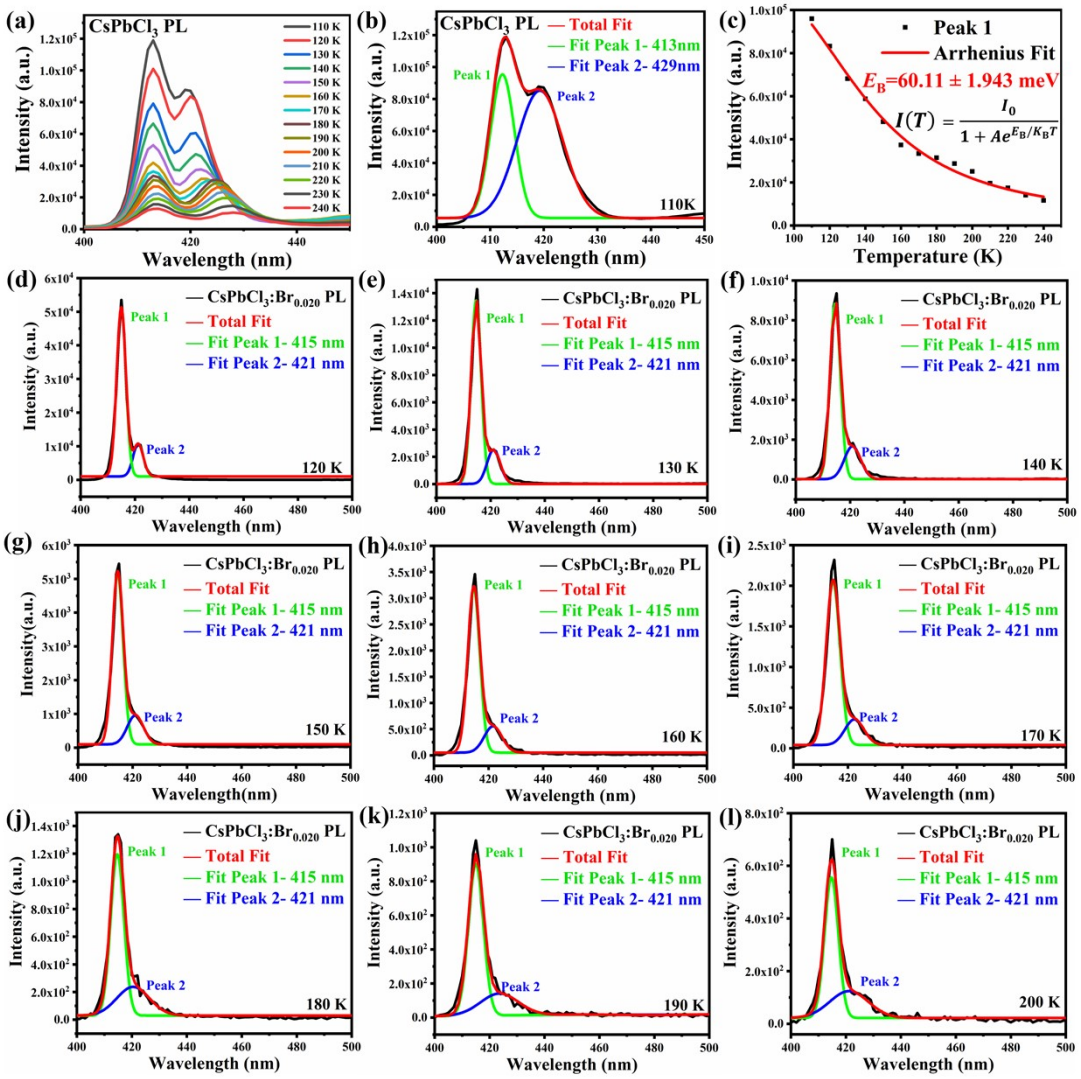

Fig. S11 (a) Temperature-dependent PL spectra from $CsPbCl_3$ crystal under excitation from a 375 nm laser with a power of 5000 μW. (b) PL spectrum collected from a cleaved sample from the $CsPbCl_3$ single crystal excited by a 375 nm laser with a power of 5000 μW at 110 K. (c) Arrhenius fitting of the evolution of PL intensity of Peak 1 with increasing temperature. (d)-(l) PL spectra collected from a cleaved sample from the $CsPbCl_3$:$Br_{0.020}$ single crystal excited by a 375 nm laser with a power of 5000 μW at 120-200 K.

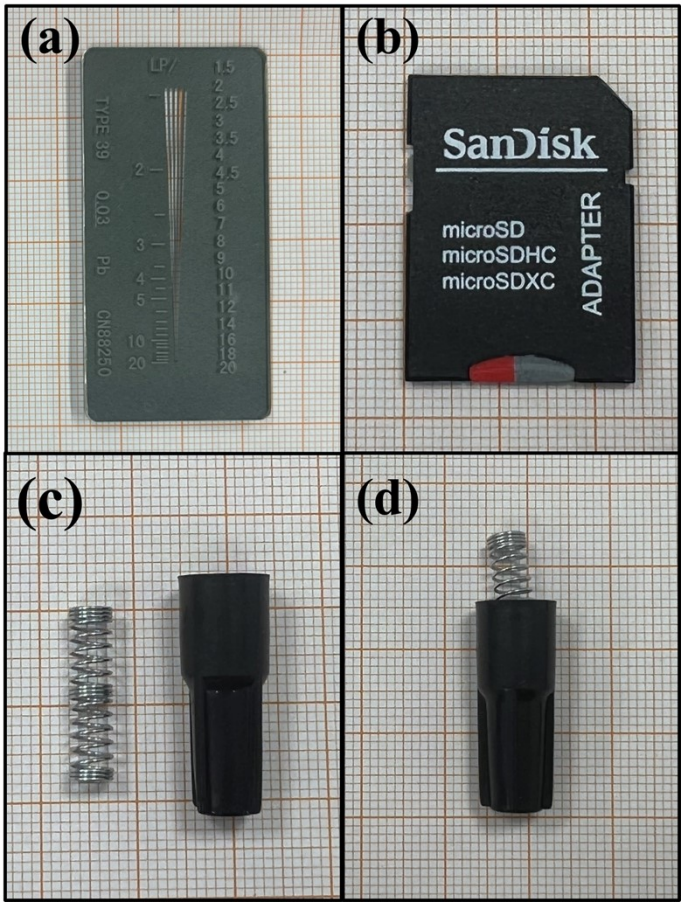

Fig. S12 X-ray imaging targets. (a) Photograph of the line pair test pattern and its spatial resolution at different areas. (b) Photograph of a memory card for imaging object. (c), (d) Photographs of a metallic spring and a black plastic shell for imaging object.

Reference

1. M. Kriechbaum, D. Otte, M. List and U. Monkowius, *Dalton Trans.*, 2014, **43**, 8781-8791.
2. D. C. Baynton, *Rev. Am. Hist.*, 2002, **30**, 227-235.
3. M. Iwanaga, *Phase Transit.*, 2005, **78**, 377-385.
4. H.M. Rietveld, *J. Appl. Crystallogr.,* 1969, **2**, 65-71.
5. E. H. Sujiono, V. Zharvan, S. A. Poetra, M. Muchtar, A. M. Idris and M. Y. Dahlan, *Mater. Today: Proc.*, 2021, **44**, 3381-3384.
6. S. Cheng, X. Zheng, Z. Hou, R. Hu, S. Jiang, S. Xi, G. Wen and X. Liu, *J. Mater. Chem. C*, 2022, **10**, 5693-5706.
7. E. Van Loef, P. Dorenbos, C. Van Eijk, K. Krämer and H. Güdel, *Appl. Phys. Lett. 2*, 2001, **79**, 1573-1575.
8. Yamamoto, S.; Ishibashi, H. *IEEE Trans. Nucl. Sci.* 1998, **45**, 1078–1082.
9. Lewellen, T.K., *Phys. Med. Biol.,* 2008, **53**, R287.
10. W. W. Moses and S. Derenzo, *IEEE Trans. Nucl. Sci.*, 1999, **46**, 474-478.
11. Kinahan, P.E.; Townsend, D.W.; Beyer, T.; Sashin, D., *Med. Phys.* 1998, **25**, 2046–2053.
12. G. A. Appleby, J. Zimmermann, S. Hesse and H. von Seggern, *J. Appl. Phys.*, 2011, **109,** 013507.